THE ASTRONOMICAL JOURNAL, 115:460–471, 1998 February

HIGH-IONIZATION NUCLEAR EMISSION-LINE REGION IN THE SEYFERT GALAXY TOLOLO 0109−383

TAKASHI MURAYAMA AND YOSHIAKI TANIGUCHI[1]
Astronomical Institute, Tohoku University, Aoba, Sendai 980-77, Japan; murayama@astroa.astr.tohoku.ac.jp, tani@astroa.astr.tohoku.ac.jp
AND
KAZUSHI IWASAWA[1]
Institute of Astronomy, University of Cambridge, Madingley Road, Cambridge, CB3 0HA, England, UK; ki@ast.cam.ac.uk
Received 1997 July 31; revised 1997 October 20

ABSTRACT

We present a detailed optical spectroscopic analysis of the high-ionization Seyfert galaxy Tololo 0109−383, which was classified originally as a type 2 Seyfert nucleus. The high-ionization nuclear emission-line region (HINER) (traced by e.g., [Fe X] λ6374) of this galaxy is found to be spatially extended. Although the total radial extent of the HINER amounts to ∼1.1 kpc, ∼70% of the HINER emission is concentrated in the inner 220 pc in radius. The inner HINER in Tololo 0109−383 can be interpreted by the photoionization model of Ferguson, Korista, & Ferland, while the extended HINER suggests that low-density interstellar medium is also photoionized by high-energy continuum emission as described by Korista & Ferland.

We find an extended low-ionization emission line region traced by Hα, [N II], and [S II] emission lines with very narrow widths (<200 km s^{-1}) at ∼2.2 kpc east of the nucleus. This region is characterized by (1) the observed [N II]/Hα ratio, which is ∼0.8; (2) no measurable [O III] emission; and (3) a low ionization parameter, $U \sim 6 \times 10^{-5}$. These properties can also be interpreted in terms of a photoionization model.

As well as confirmation of the presence of broad emission in both Hα and Hβ lines, we also find optical Fe II emission features in our spectra. Since the optical Fe II emission is one of the important characteristics of type 1 active galactic nuclei, it is shown that Tololo 0109−383 harbors a type 1 central engine in its nucleus. Since the soft X-ray–to–infrared (60 μm) luminosity ratio of Tololo 0109−383 is higher than those of typical type 2 Seyfert nuclei, we consider that blocking by a dusty torus may be incomplete and thus we are able to observe the type 1 nature of Tololo 0109−383.

Key words: galaxies: nuclei — galaxies: Seyfert

1. INTRODUCTION

It is known that about 40% of Seyfert galaxies show high-ionization emission lines (ionization potential ≥100 eV), such as [Fe VII] λ6087, [Fe X] λ6374, [Fe XI] λ7892, and [Fe XIV] λ5303, (Oke & Sargent 1968; Grandi 1978; Penston et al. 1984; De Robertis & Osterbrock 1986). Since these high-ionization lines are also seen in the solar corona and were originally thought to arise from high-temperature ($T > 10^5$ K) regions around active galactic nuclei (AGNs), they have been often referred as coronal lines (Oke & Sargent 1968). However, there has been controversy regarding the origin of these emission lines (see below), and thus it is still uncertain whether the high-ionization lines come from regions with coronal temperatures. Therefore, in this paper, we use the term high-ionization nuclear emission-line region (HINER) instead of coronal line region (CLR). HINER is a good physical contrast to LINER (low-ionization nuclear emission-line region; Heckman 1980).

There has been debate about the origin of the high-ionization lines. The possible origins are summarized as follows: (1) a hot, collisionally ionized gas with temperatures of $T_e \sim 10^6$ K (Oke & Sargent 1968; Nussbaumer & Osterbrock 1970); (2) a cool gas ($T_e \sim$ a few times 10^4 K and $n_e \sim 10^6$ cm^{-3}) photoionized by the central nonthermal continuum emission (Osterbrock 1969, 1981; Nussbaumer & Osterbrock 1970; Grandi 1978); (3) a low-density (e.g., $n_e \sim 1$ cm^{-3}) interstellar medium (ISM) photoionized by the central nonthermal continuum emission (Korista & Ferland 1989; hereafter KF89); or (4) a combination of shocks and photoionization by the central nonthermal continuum emission (Viegas-Aldrovandi & Contini 1979). See Ferguson, Korista, & Ferland (1997) for a recent detailed study of the physical conditions of HINERs based on photoionization simulations.

HINERs tend to show intermediate properties between broad-line regions (BLRs) and narrow-line regions (NLRs). For example, emission-line widths of HINERs are systematically broader than those of low-ionization forbidden lines (De Robertis & Osterbrock 1984, 1986; Osterbrock 1981; Osterbrock & Pogge 1985; Penston et al. 1984). It is also known that the high-ionization lines are systematically blueshifted to the low-ionization lines, e.g., $\simeq -200$ km s^{-1} (e.g., Grandi 1981). Further, Veilleux (1991) presented evidence for the large blueward asymmetry in high-ionization lines of a type I Seyfert galaxy Mrk 359. Since the high-ionization lines have higher critical densities ($n_{cr} \sim 10^7$ to 10^{10} cm^{-3}), it is likely that HINERs reside in the inner part of the NLRs (e.g., Osterbrock 1969; Oliva et al. 1994) or near the surface of the molecular/dusty tori irradiated by the central engine (Pier & Voit 1995). If this is the case, the HINER would come from a very compact region near the nuclei. In fact, recent optical and near-infrared spectro-

[1] Visiting Astronomer, Cerro Tololo Inter-American Observatory, National Optical Astronomy Observatories, operated by the Association of Universities for Research in Astronomy, Inc., under cooperative agreement with the National Science Foundation.

scopic studies of the high-ionization lines of AGNs show that the HINERs are very compact ($\simeq 10$ pc) with a density of $\sim 10^2$ cm^{-3} (Oliva et al. 1994; Marconi et al. 1994). On the other hand, Golev et al. (1994) show that the HINER in the Seyfert galaxy NGC 3516 is spatially extended (several kpc), which is consistent with the photoionization model proposed by KF89. The above observations suggest that the major site of HINERs may be different from AGN to AGN. This makes it difficult to obtain a comprehensive understanding of HINERs.

Since most of the previous studies have been based on aperture spectrophotometry, it is difficult to study spatial structures of HINERs. In this paper, we describe our long-slit spectroscopy of the well-known high-ionization Seyfert galaxy Tololo 0109−383 (=NGC 424 = ESO 296-4; Smith 1975; Lauberts 1982). Since the apparent luminosity of the HINER of this galaxy is the brightest among nearby Seyfert nuclei (Fosbury & Sansom 1983, hereafter FS83; Durret & Bergeron 1988, hereafter DB88; Durret 1990), this galaxy is very suitable for a detailed study of HINER. Another interesting property of Tololo 0109−383 is that its nucleus exhibits marginal properties between type 1 and 2 Seyfert nuclei. Although Tololo 0109−383 was originally classified as type 2 Seyfert (Smith 1975), Boisson & Durret (1986) found that the reddening-corrected ultraviolet–to–near-infrared continuum spectrum of Tololo 0109−383 is almost flat and is quite similar to those of Seyfert 1 nuclei. They also found the broad component in the Hα emission. These observational properties led them to conclude that Tololo 0109−383 has an *obscured* type 1 Seyfert nucleus. Durret (1990) noted that Tololo 0109−383 is a unique object among the candidates of obscured type 1 Seyfert nuclei, because only this galaxy has unusually intense high-ionization emission lines. Motivated by these interesting properties, we present our new optical spectroscopy of Tololo 0109−383.[2]

2. OBSERVATIONS

The spectroscopic observations of Tololo 0109−383 were obtained at the 1.5 m telescope of Cerro Tololo Inter-American Observatory (CTIO), National Optical Astronomy Observatories, in 1992 August and September. The 1.5 m CCD spectrometer consists of a GEC CCD detector system mounted on the f/7.5 Cassegrain spectrograph. The two gratings (Nos. 16 and 25) were used to obtain blue (4000–5500 Å) and red (6000–7000 Å) spectra. The spectral resolutions were 5.2 and 4.5 Å for the blue and the red spectral regions, respectively, with a 3″ slit. We took two sets of blue and red spectra and the total exposures were 3600 and 2100, respectively. The data were reduced with the use of IRAF. The reduction was made with a standard procedure; bias subtraction and flat fielding were made with the data of the dome flats. Flux calibration was obtained using a CTIO standard star (Hamuy et al. 1992). The observations were made in photometric conditions. The two independent spectra were stacked into one spectrum for the blue and the red regions in order to improve signal-to-noise ratios. The nuclear spectrum was extracted for each spectral region with 3″ aperture. The seeing size derived from the spatial profile of the standard star is 1″.5 (FWHM) both in the blue and red spectra.

[2] We use a distance toward Tololo 0109−383 of 45.29 Mpc, which is estimated with a recession velocity with respect to the Galactic Standard of Rest, $V_{GSR} = 3397$ km s^{-1} (de Vaucouleurs et al. 1991) and a Hubble constant of $H_0 = 75$ km s^{-1} Mpc^{-1}. At this distance, 1″ corresponds to 220 pc.

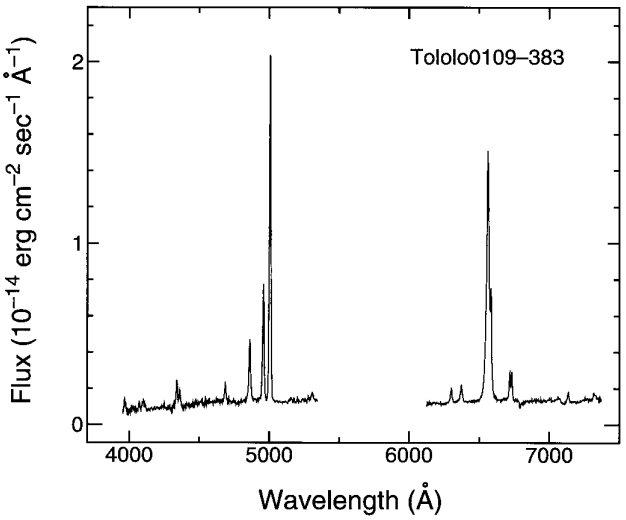

FIG. 1.—Nuclear spectrum of Tololo 0109−383

3. RESULTS

3.1. *Emission-line Properties*

The final blue and red spectra of the nuclear region are shown in Figure 1. Faint emission features are separately shown in Figure 2, which shows the presence of broad component in both Hα and Hβ emission. Further, an emission bump between Hγ and Hβ is clearly observed in the blue spectrum. It is most likely that this feature is attributed to the Fe II λ4570 blend (37 and 38). In order to estimate

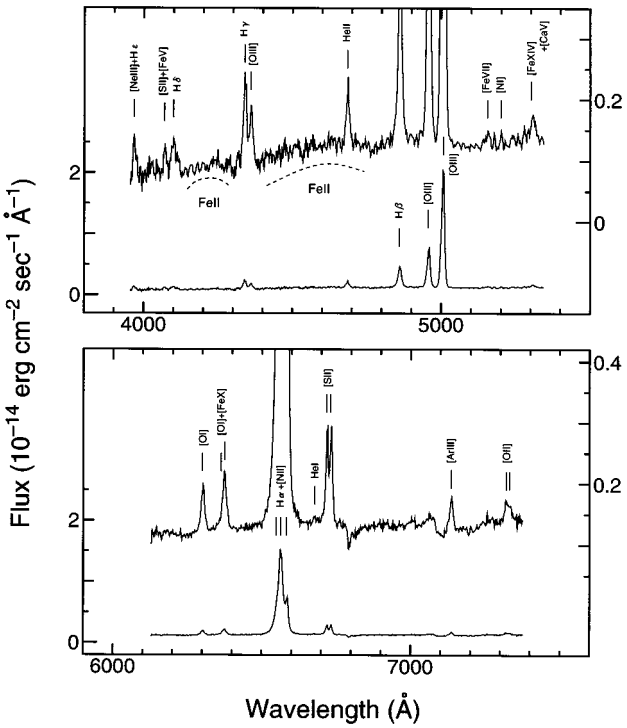

FIG. 2.—Fe II emission and other weak emission lines of Tololo 0109−383.

emission-line fluxes, we made multicomponent Gaussian fittings for both the blue and red spectra. The results are shown in Figures 3 and 4, respectively. Though the fitting residual both in the Hβ and Hα regions seems poor, adding another component (i.e., intermediate broad lines or multiple components for narrow lines) could not improve the fitting. Because increasing Gaussian components did not change the emission-line fluxes significantly, the quality of fitting does not affect the results and further discussion. In the blue spectrum, other Fe II features are also seen near the Hβ (blend 42 and 43) and Hγ (blends 27 and 28), which are identified as the components 7 and 13 in our fitting. Since the line width of the Fe II λ4570 emission seems to be very large, the measured flux of the Fe II λ4570 emission should be regarded as an upper limit. The identified emission lines are summarized in Table 1. Both the observed and the reddening-corrected intensities relative to that of Hβ narrow component are also given in Table 2. The reddening is estimated by using the Balmer decrement (the narrow component ratio of Hα/Hβ) following the usual manner described in Osterbrock (1989). Assuming an intrinsic value of Hα/Hβ ratio is 3.1 (Ferland & Netzer 1983; Ferland & Osterbrock 1985, 1986) we obtain $A_V = 1.38$ mag. This value is slightly different from the previous estimates; $A_V =$ 1.6 mag (FS83) and 2.01 mag (DB88). It is noted that the reddening is typical for type 2 Seyfert Galaxies ($\sim$1.1 mag; Dahari & De Robertis 1988). The [O III] λ5007 emission-line width (460 km s^{-1}) is close to a median value of type 2 Seyfert galaxies (510 km s^{-1}; Feldman et al. 1982).

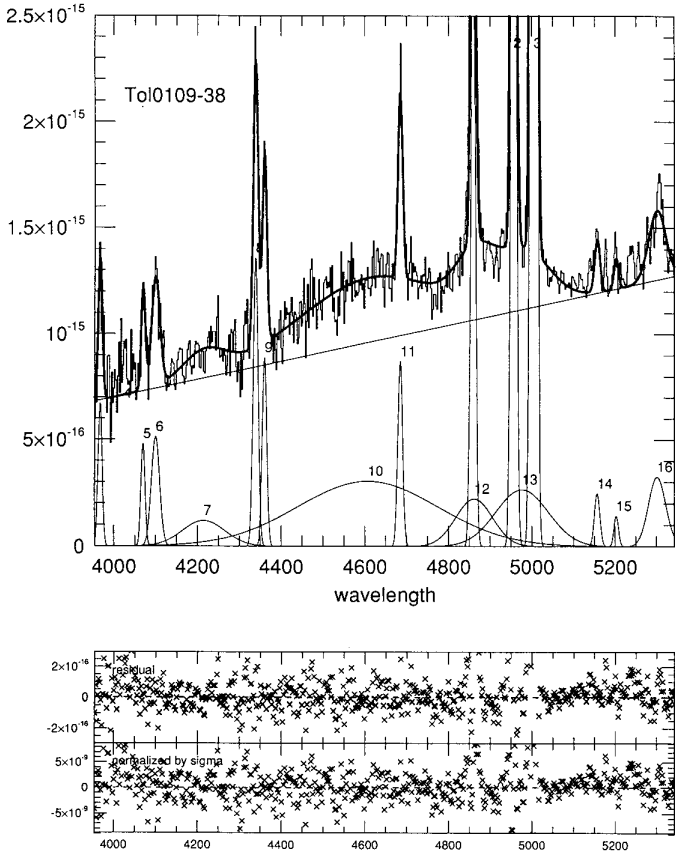

FIG. 3.—Result of multi-Gaussian component analysis for the blue spectrum of Tololo 0109−383. The Fe II λ4570 emission corresponds to the feature No. 10. The broad component of Hβ emission is No. 12. Fitting was made with LDECONV developed by Michitoshi Yoshida.

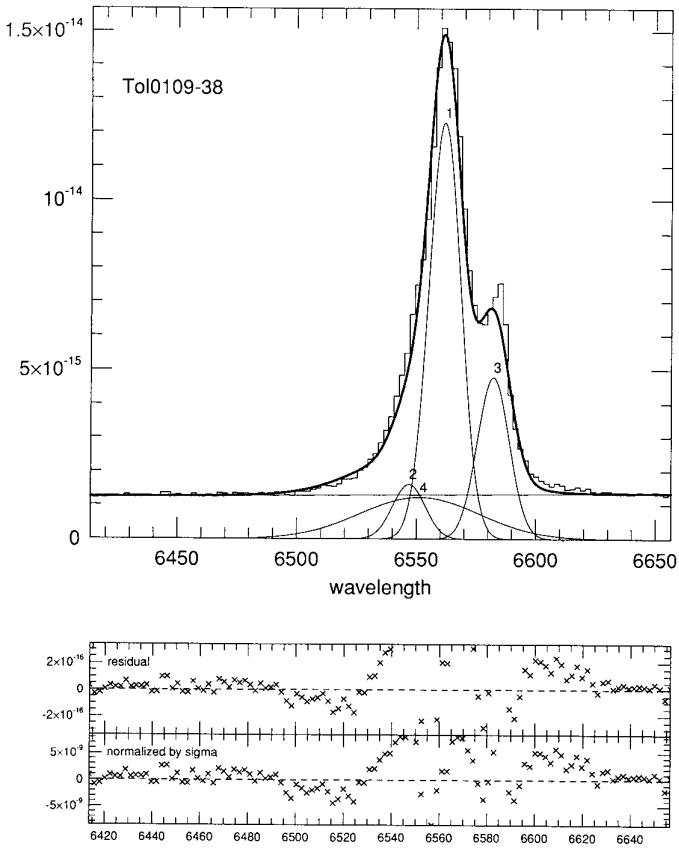

FIG. 4.—Result of multi-Gaussian component analysis for the Hα + [N II] emission lines of Tololo 0109−383. The broad Hα component is No. 4.

Tololo 0109−383 was originally classified as a type 2 Seyfert galaxy because of the absence of broad line emission (FS83).[3] However, Boisson & Durret (1986) found the broad component in the Hα emission. In Table 2, we give a comparison between our results and the previous observations (FS83; Boisson & Durret 1986; DB88). Boisson & Durret (1986) and DB88 used the same data taken with the ESO 3.6 m telescope. Boisson & Durret (1986) gave a brief comment on the discovery of the broad Balmer component, and DB88 gave their detailed analysis. The relative strength of the broad Hα component in DB88 is significantly larger than ours. Since our slit width (3″) is wider than theirs (2″), it is possible that the relative strength of the broad component in our measurement is weaker than theirs. However, we cannot rule out another possibility of time variation because the BLR emission indicates frequently significant time variations both in the flux and in the profile shape (e.g., Peterson 1993).

The high-ionization Seyfert galaxies tend to show few or no optical Fe II emission lines (Osterbrock 1981; see, however, Kunth & Sargent 1979). However, as well as the confirmation of the presence of broad emission, our finding of the Fe II emission supports the type 1 nature of Tololo 0109−383, because the optical Fe II emission lines are considered to arise from warm neutral zone (e.g., $T_e \simeq 10^4$ K and $n_{H0}/n_{H+} \simeq 10$) in the BLR (Phillips 1978a, 1978b; Joly 1991). The dereddened Fe II λ4570/Hβ_{broad} ratio, $\sim$3.5, is

[3] Although the trace of broad Hα component in the spectrum in FS83 can be seen, they did not mention the broad component.

TABLE 1

EMISSION-LINE DATA

Identification	λ_{obs} (Å)	λ_{rest} (Å)	FWHM[a] (km s^{-1})	$F/F(H\beta\ N)$[b]	$I/I(H\beta\ N)$[c]
[Ne III] + Hε	4013.6	3969.3	338	0.202	0.273
[S II] + [Fe V].....	4117.1	4071.6	341	0.147	0.192
Hδ.....	4147.4	4101.6	938	0.314	0.407
Fe II?	4263.8	4216.7	5069	0.373	0.466
Hγ.....	4389.5	4341.0	441	0.492	0.589
[O III]	4410.9	4362.2	386	0.299	0.356
Fe II.....	4660.9	4609.4	15392	3.178	3.509
He II	4739.3	4687.0	389	0.307	0.328
Hβ N	4915.6	4861.3	348	1.000	1.000
Hβ B.....	4918.5	4864.2	3833	0.610	0.610
[O III]	5014.4	4959.0	341	2.038	1.963
[O III]	5062.9	5007.0	338	6.014	5.683
Fe II?	5034.6	4979.0	5326	1.036	0.990
[Fe VII]	5216.8	5159.2	437	0.099	0.088
[N I]	5263.4	5205.3	330	0.049	0.042
[Fe XIV]	5363.3	5304.1	1638	0.423	0.356
[O I]	6373.8	6301.8	405	0.292	0.187
[O I]	6438.0	6365.4	401	0.097	0.061
[Fe X]	6448.7	6375.9	349	0.302	0.190
[N II]	6623.2	6548.5	383	0.679	0.410
Hα N	6638.2	6563.3	382	5.155	3.100
Hα B.....	6627.8	6553.0	1582	1.896	1.143
[N II]	6658.9	6583.8	381	2.003	1.201
He I	6754.3	6678.1	210	0.039	0.023
[S II]	6795.8	6719.2	209	0.415	0.244
[S II]	6810.4	6733.6	208	0.422	0.247
[Ar III].....	7217.8	7136.4	301	0.185	0.101
[O II]	7405.2	7321.7	336	0.107	0.057
[O II]	7416.4	7332.7	335	0.064	0.034

[a] Corrected for the instrumental width.
[b] $F(H\beta\ N) = 4.00 \times 10^{-14}$ ergs s^{-1} cm^{-2}.
[c] The reddening-corrected relative intensities.

quite large, because most of the Seyfert 1 galaxies have ratios less than 1 (cf. Joly 1991). Since the so-called extreme Fe II emitters have the observed ratios ranging from 2 to 6 (Bergeron & Kunth 1980; Lawrence et al. 1988; Lipari, Terlevich, & Macchetto 1993), we consider that Tololo 0109−383 belongs to a class of the extreme Fe II emitters, although its absolute flux is much lower than those of the previously known extreme Fe II emitters.

In our blue spectrum, a weak emission line is detected at λ5304.1 in the rest frame. This emission feature was pre-

TABLE 2

A COMPARISON OF OUR DATA WITH PREVIOUS DATA

	FS83[a]	BD86[b]	DB88[c]	Ours
Date	77-07-21	78-09-04	78-09-04	92-08-31
Telescope	AAT 3.9 m	ESO 3.6 m	ESO 3.6 m	CTIO 1.5 m
Detector.....	IPCS	IPCS	IPCS	CCD
Slit width (arcsec)	1.0	2.0	2.0	3.0
Flux (10^{-14} ergs s^{-1} cm^{-2}):				
$F(H\beta\ N)$	2.50[d]	...	5.80	4.00
$F(H\beta\ B)$	0.0	...	3.30	2.44
$F(H\alpha\ N)$	24.6[d,e]	...	39.1	20.6
$F(H\alpha\ B)$	0.0	...	31.0	7.58
$F(H\alpha\ N)/F(H\beta\ N)$	9.84	...	6.74	5.16
$F(H\alpha\ B)/F(H\beta\ B)$	...	6.8	9.39	3.11
$F(H\beta\ N)/F(H\beta\ B)$	...	...	1.76	1.64
$F(H\alpha\ N)/F(H\alpha\ B)$.....	...	...	1.26	2.72
FWHM (km s^{-1})				
Hα B.....	...	1800	...	1582
Hβ B.....	...	1800	...	3883
A_V (mag)	1.6	...	2.01	1.38

[a] Fosbury & Sansom 1983.
[b] Boisson & Durret 1986.
[c] Durret & Bergeron 1988.
[d] This value should be increased by between 25% and 100% because of the difference in slit size between the galaxy and the standard star.
[e] The contribution of [N II] λλ6548, 6584 emission is included in this flux.

viously assigned as [Fe XIV] λ5303 or [Ca V] λ5309 (cf. FS83). This feature was also observed in other high-ionization Seyfert galaxies, such as III Zw 77 (Osterbrock 1981; Alloin et al. 1992). Since the rest wavelength measured here (5304.1 Å) is much closer to [Fe XIV] λ5303 than to [Ca V] λ5309, the identification of [Fe XIV] seems more probable for the case of Tololo 0109−383. Therefore, we will refer this line as [Fe XIV] below. However, the line width is significantly broader than those of other emission lines; we cannot rule out some contribution of the [Ca V] λ5309 emission.

Finally, we investigate the ionization and the density structure of the HINER, as well as the NLR in Tololo 0109−383. It is known that the positive correlation between FWHM and n_{cr} is found particularly for type 2 Seyfert nuclei while that between FWHM and ionization potential for type 1s (Pelat, Alloin, & Fosbury 1981; Fillpenko 1985; De Robertis & Osterbrock 1984, 1986; Osterbrock 1989). This difference may be interpreted as due to the difference of the gas density distribution in NLRs between type 1 and 2 Seyfert nuclei (e.g., Osterbrock 1989); there is little radial variation of electron density in the NLRs of type 1's while $n_e \propto r^{-2}$ for type 2's. Although this difference has not yet been fully understood, it may be due to the orientation effect; i.e., the NLRs of type 1's are systematically viewed from pole-on, while those of type 2's are viewed from edge-on (Schmitt & Kinney 1996). First we study a correlation between FWHM and critical density (n_{cr}) for the collisionally excited emission lines. In Figure 5, we show the diagram of FWHM versus n_{cr} for Tololo 0109−383 and III Zw 77, which is one of the highest ionization Seyfert 1 galaxies (Osterbrock 1981). Positive correlations are found for both the galaxies, while the correlation is better for III Zw 77 than for Tololo 0109−383. Next, we show a diagram of FWHM versus ionization potential for both the galaxies in Figure 6. Although there is a significant, positive correlation for III Zw 77, there is little correlation for Tololo 0109−383, particularly for the emission lines with ionization potentials of 0–250 eV. Since the both correlations for Tololo 0109−383 are relatively poor, the density and ionization structure in this galaxy is not interpreted in a simple way.

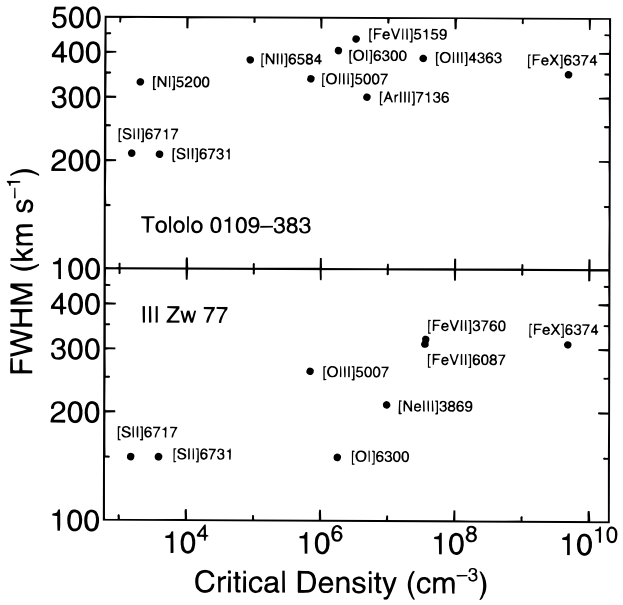

FIG. 5.—Diagram of FWHM (km s^{-1}) vs. critical density, n_{cr} (cm^{-3}), for the forbidden emission lines for Tololo 0109−383 (*top*) and III Zw 77 (*bottom*).

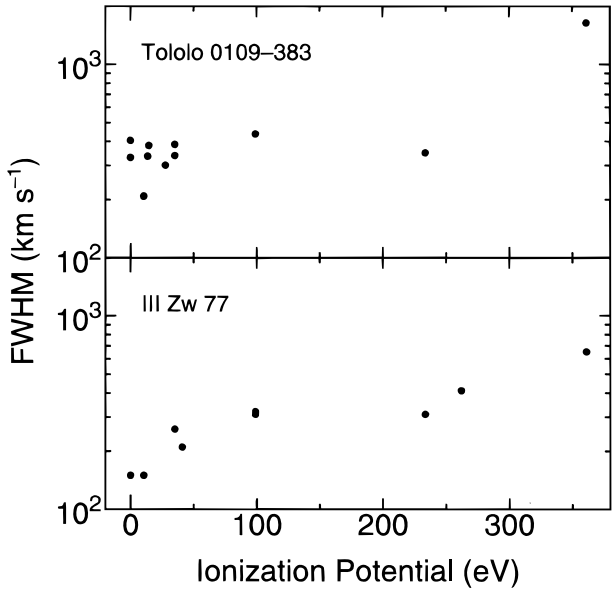

FIG. 6.—Diagram of FWHM (km s^{-1}) vs. ionization potential for the forbidden emission lines for Tololo 0109−383 (*top*) and III Zw 77 (*bottom*).

3.2. *Spatial Distribution of the Emission-Line Regions*

In order to understand the origin of HINERs in Seyfert nuclei, it is crucial to study spatial structures of the HINERs in detail. If high-ionization lines such as [Fe XIV], [Fe X], and [Fe VII] arise either from inner parts of the NLR (cf. Osterbrock 1969; Grandi 1978; Penston et al. 1984; Oliva et al. 1994; Ferguson et al. 1997) or from an inner surface of molecular/dusty tori (Pier & Voit 1995), the HINERs would be observed just near the nuclei. On the other hand, if the HINERs arise from the low-density ISM photoionized by the central continuum source, their geometric sizes become of order 1 kpc, and thus the HINERs would be resolved spatially (KF89; Golev et al. 1994).

First, we show the slit profiles of the emission lines together with those of the blue and red continuum emission in Fig. 7. Their spatial extents (FWHM both in arcseconds and parsecs) are summarized in Table 3. The values of FWHM scatter from 500 pc (Hβ, [O III], the blue continuum) to 800 pc (He II, [O I], Hα + [N II], and so on). However, there is no tendency that the higher-ionization emission lines have centrally concentrated distribution. The red continuum has a wider FWHM than the blue one. This may be due to the effect of red stars in the nuclear bulge because the host galaxy of Tololo 0109−383 is an early-type (Sa) disk galaxy (Smith 1975; Durret & Bergeron 1987).

In order to see more detailed spatial distributions of the emission-line region, we show continuum-subtracted images of some bright and interesting emission lines in Fig. 8. The most remarkable line is [Fe X] λ6374, because it is more extended than the other low-ionization lines. Since the wavelength of [Fe X] λ6374 is close to that of [O I] λ6364, these two emission lines are observed as a single emission component in our spectrum. The strength of [O I] λ6364 is one-third of that of [O I] λ6300 (Osterbrock 1989). Since,

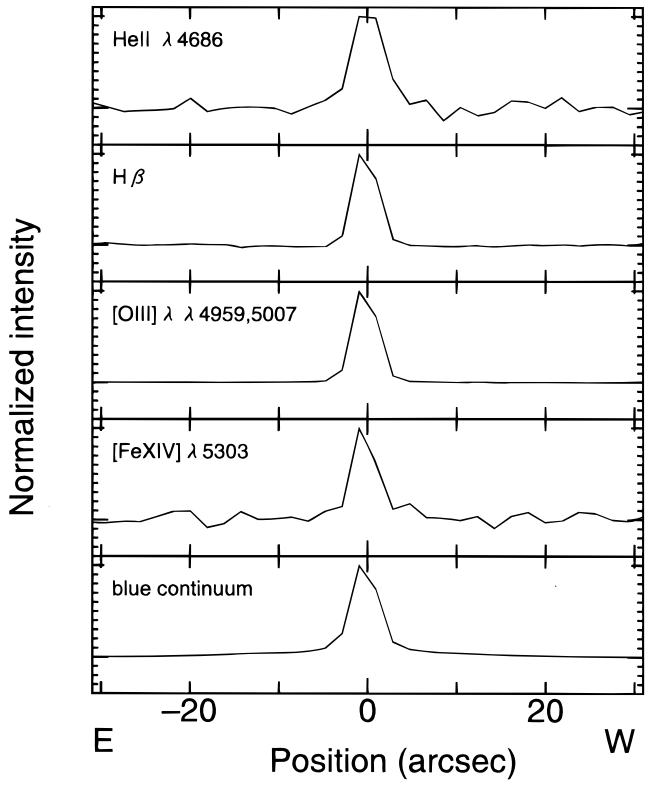

FIG. 7a

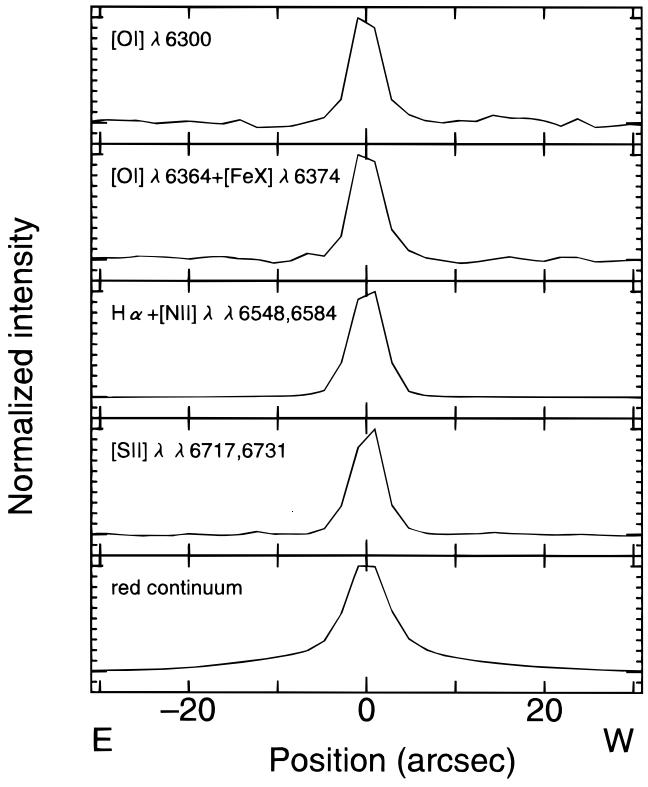

FIG. 7b

FIG. 7.—Spatial extent (slit profile) of emission-line and continuum emission regions: (*a*) blue spectral region and (*b*) red spectral region

TABLE 3

SPATIAL SIZES OF THE CONTINUUM AND EMISSION-LINE REGIONS

Emission	FWHM[a] (arcsec)	FWHM[a] (pc)
Blue spectral region:		
He II λ4686	3.88	853
Hβ λ4861	2.20	484
[O III] λ4959, 5007	2.26	497
[Fe XIV] λ5303	2.28	502
Blue continuum[b]	2.56	563
Red spectral region:		
[O I] λ6300	3.27	719
[O I] λ6364 + [Fe X] λ6374	3.46	761
Hα λ6563 + [N II] λλ6548, 6584	3.92	862
[S II] λλ6717, 6731	3.61	794
Red continuum[c]	3.46	761

[a] Corrected for the seeing size.
[b] Blue continuum: λ5110–λ5170 in the observed frame.
[c] Red continuum: λ6490–λ6550 in the observed frame.

however, the strength of [O I] λ6364 + [Fe X] λ6374 emission feature is almost comparable to that of [O I] λ6300, it turns out that the [Fe X] emission is fairly strong in the central ±3″ nuclear region. Figure 9 shows the spatial variation of [O I] λ6300, 6364 and [Fe X] λ6374 emission-line features in detail. Assuming F([O I] λ6364) = F([O I] λ6300)/3, we estimate the flux contribution of the [Fe X] λ6374 emission (Table 4). There is a tendency that the [Fe X]–emitting region is more intense in the western direction. It is remarkable that the [Fe X] emission line can be seen, while the [O I] λ6300 emission seems to disappear even in both the 4″.8 west and 4″.8 east regions. Namely, the [Fe X] emitting region is extended up to 5″ in radius (corresponding to 1.1 kpc), being more extended than the NLR traced by [O I]. It is, however, noted that about 67% of the total [Fe X] emission comes from the inner 2″ (440 pc) region in diameter (see Table 4). In conclusion, the [Fe X]–emitting region is concentrated mostly in the

TABLE 4

SPATIAL VARIATION OF THE ([O I] λ6364 + [Fe X] λ6374)/[O I] λ6300 RATIO

Position (arc sec)	F([O I] λ6300) (10^{-15} ergs s^{-1} cm^{-2})	F([O I] λ6364 + [Fe X] λ6374) (10^{-15} ergs s^{-1} cm^{-2})	F([Fe X] λ6374)[a] (10^{-15} ergs s^{-1} cm^{-2})
E4.8	<0.47[b]	1.46 ± 0.14	1.3[c]
E2.9	2.31 ± 0.17	2.57 ± 0.18	1.8
E1.0	6.73 ± 0.15	8.20 ± 0.17	6.0
W1.0.....	5.94 ± 0.16	8.61 ± 0.18	6.6
W2.9.....	1.62 ± 0.12	2.89 ± 0.19	2.4
W4.8.....	<0.35[b]	0.92 ± 0.14	0.8[c]

[a] F([Fe X] λ6374) = F([O I] λ6364 + [Fe X] λ6374) − F([O I] λ6300)/3.
[b] 3 σ upper limit.
[c] Lower limit.

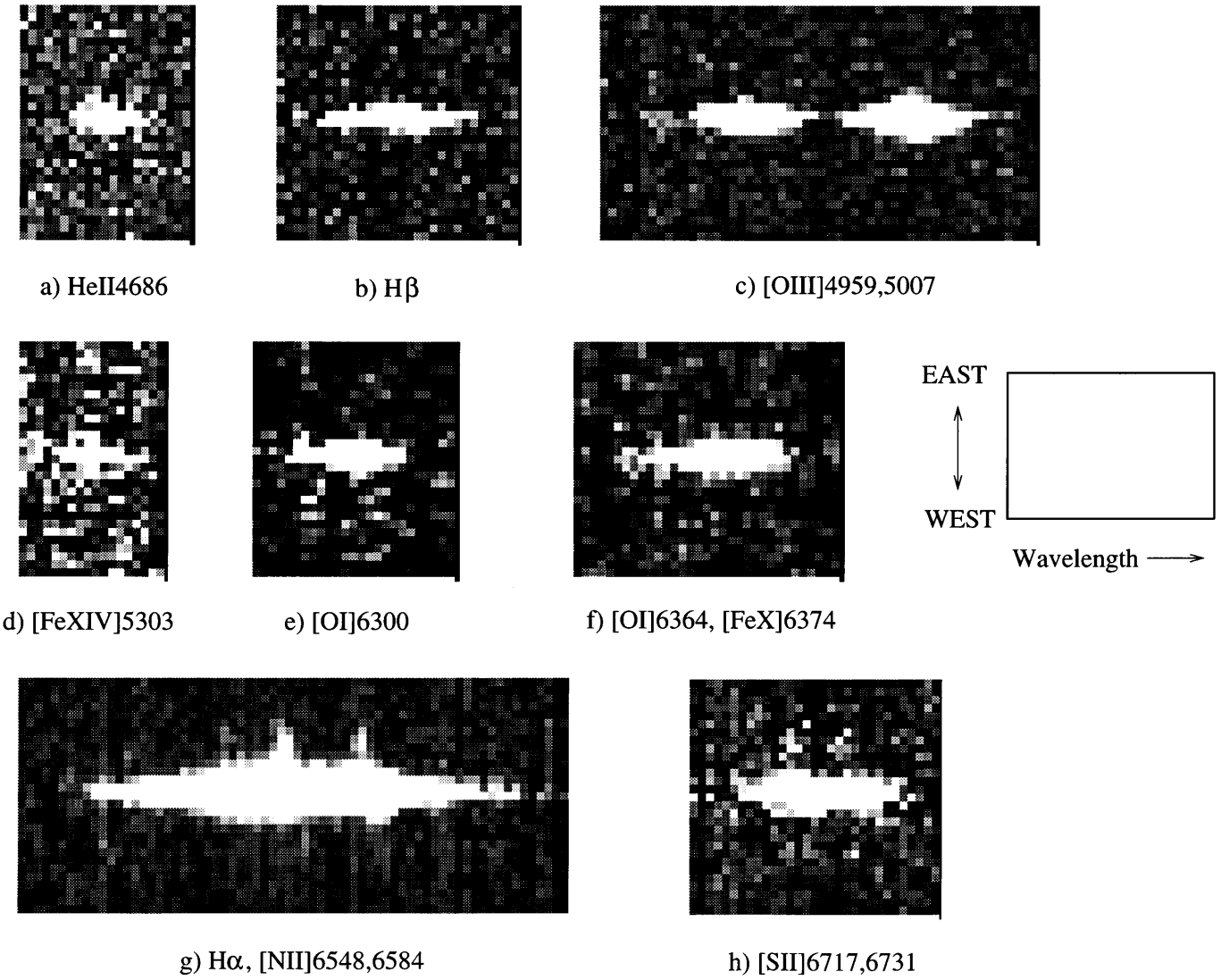

FIG. 8.—Continuum-subtracted emission-line images: (*a*) He II λ4686; (*b*) Hβ; (*c*) [O III] λ4959, 5007; (*d*) [Fe XIV] λ5303; (*e*) [O I] λ6300; (*f*) [O I] λ6364 + [Fe X] λ6374; (*g*) Hα + [N II] λ6548, 6583; and (*h*) [S II] λ6717, 6731. The extended emission-line region is seen in the Hα and [N II] emission-line image around 11″ east of the nucleus.

central several 100 pc region while extended to a radius of ~1 kpc. This result implies that the HINER in Tololo 0109−383 is *not* an intermediate region between the NLR and BLR. Our result is basically consistent with the model proposed by KF89 in which the HINERs arise from ISM photoionized by the central continuum emission. The observed [S II] doublet ratio in the central ±3″ region, [S II] λ6717/[S II] λ6731 ~ 1, yields $n_e \simeq 600[T_e/(10^4\ \mathrm{K})]^{1/2}$ cm^{-3}. On the other hand, we can see that the [S II] λ6731 intensities are fairly weaker than those of [S II] λ6717 ones at ±4″.8 region from the nucleus (see Fig. 9), suggesting $n_e \ll 100\ \mathrm{cm}^{-3}$. Therefore we consider that the outer HINER in Tololo 0109−383 is interpreted well by KF89 models.

3.3. *An Eastern Low-Ionization Emission-Line Region*

In Figure 8*g*, we find an extended emission-line region around 11″ east from the nucleus. In Figure 10, we show the blue and red spectra of this eastern emission-line region that are extracted with a 3″.8 (≃840 pc) aperture at 11″ east from the nucleus. The very narrow Hα [N II], and [S II] emission lines are seen evidently in the red spectrum, although there is no significant emission line in the blue spectrum, suggesting that the ionization level is quite low. The observed fluxes of the detected emission lines are given in Table 5. Given that the [N II]/Hα ratio is ~0.8 and that there is no measurable [O III] emission, this emission-line region is classified as a LINER (Heckman 1980; Veilleux & Osterbrock 1987).

In order to study the ionization in this region, we estimate an ionization parameter, U (the ratio of ionizing photon density to the eletron density). First we estimate the

TABLE 5

SPECTRAL PROPERTIES OF THE EXTENDED EASTERN EMISSION-LINE REGION

Identification	λ_{obs} (Å)	FWHM (km s^{-1})	$F/F(\mathrm{H}\alpha)$[a]
[N II] λ6548.....	6621.0	<200	0.267
Hα.....	6635.9	<200	1.000
[N II] λ6584.....	6656.7	<200	0.788
[S II] λ6717	6791.1	<200	0.338
[S II] λ6731	6805.7	<200	0.275

[a] $F(\mathrm{H}\alpha) = 1.27 \times 10^{-15}$ ergs s^{-1} cm^{-2}.

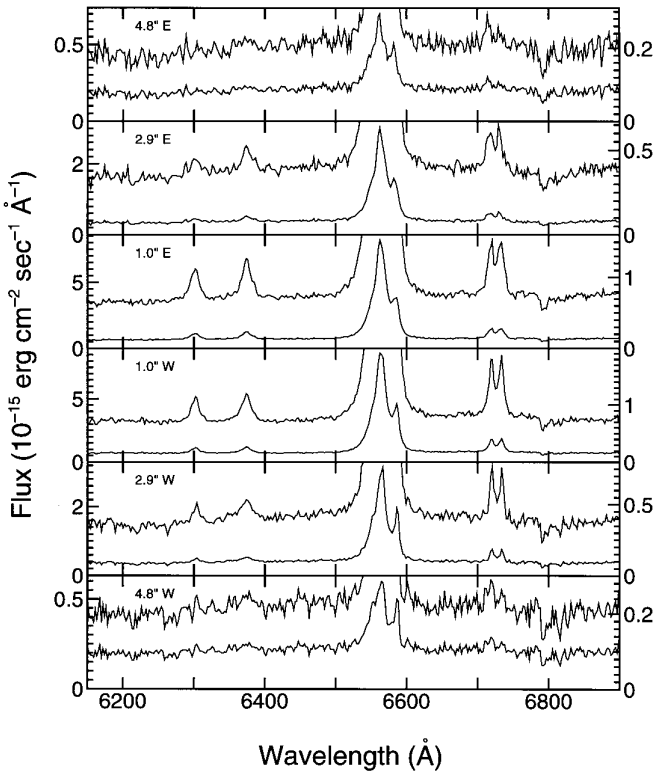

FIG. 9.—Profile variations of the [O I] λ6300 and [O I] λ6364 + [Fe X] λ6374 emission lines along the slit.

number of the ionizing photons. The Hα flux, 1.27×10^{-15} ergs cm^{-2} s^{-1}, integrated over the area of 3.″8 × 3.″0 (=840 pc × 660 pc) gives the Hα luminosity, $L_{H\alpha} \simeq 3.12 \times 10^{38}$ ergs s^{-1}, giving the number of Hα photons, 1.03×10^{50} photons. Since 2.2 ionizing photons produce an Hα photon (Osterbrock 1989), the number of ionizing photons derived from this Hα luminosity is $Q \simeq 2.3 \times 10^{50}$ photons s^{-1}. The observed [S II] doublet ratio, [S II] λ6717/[S II] λ6731 = 1.23 ± 0.17, gives an electron density, $n_e \simeq 200\ [T_e/(10^4\ \mathrm{K})]^{1/2}$ cm^{-3}, where T_e is the electron temperature (Osterbrock 1989). However, regarding the error of the [S II] ratio, we cannot exclude the possibility that the electron density is much smaller than the value above, because the [S II] doublet ratio is close to the low density limit value. The ionization parameter can be estimated as $U = Q/(Scn_e)$ where c is the light velocity and S is the total area of emission-line region irradiated by the central engine. This area can be given by $S = w \times (660\ \mathrm{pc})$, where w is the thickness of the emission-line region in the line of sight. Then we derive $U \sim 6 \times 10^{-5}[w/(100\ \mathrm{pc})]^{-1}$. Although there is an uncertainty in the thickness, w, this ionization parameter may be smaller than typical values for LINERs ($\sim 10^{-3}$–10^{-4}: cf. Ferland & Netzer 1983; Osterbrock 1989). But, as we stated above, if the electron density is significantly smaller than 200 cm^{-3}, the ionization parameter will be a typical value.

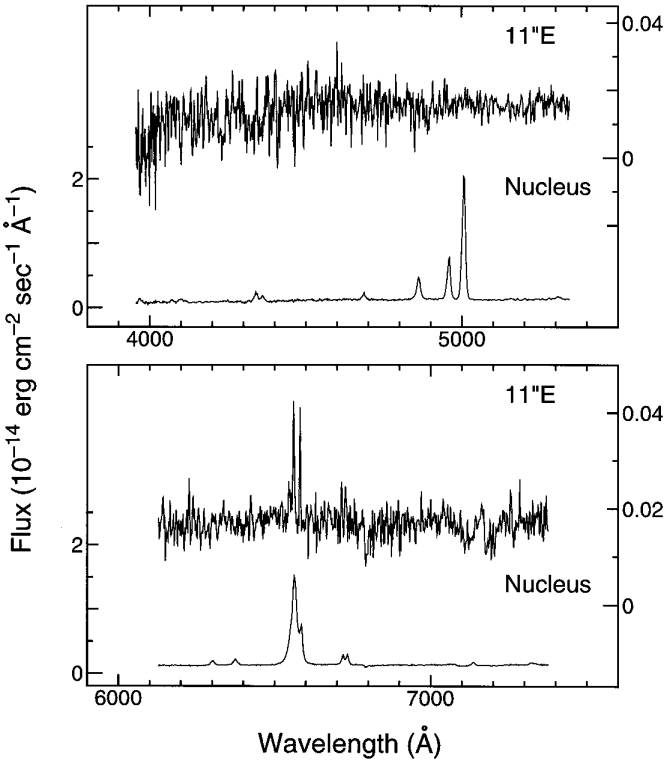

FIG. 10.—Blue and red spectra of the eastern low-ionization emission-line region. The nuclear spectra are also shown for reference.

This extranuclear emission-line region is observed in the direction at which the [Fe X] emission is weaker. Along this direction, there is a pair of radio continuum jets (Ulvestad & Wilson 1989). The eastern radio component is also weaker than the western one. This suggest that the non-thermal continuum emission from the nucleus has the two favored directions with different quality and/or quantity of the continuum emission. This difference may be due to the asymmetrical distribution of the gas and dust contents in the circumnuclear region of Tololo 0109−383.

4. DISCUSSION

4.1. *Where is the HINER in AGN?*

One of the most important questions about the HINERs is their location. There are three alternatives: (1) the inner surface of molecular/dusty tori (Pier & Voit 1995); (2) the inner regions of NLRs (Ferguson et al. 1997); or (3) the outer regions of NLRs or the low-density ISM in the circumnuclear region (KF89). The first two cases imply that the HINERs are centrally concentrated in the nuclear regions. Since the typical inner radii of tori in Seyfert nuclei are ∼1 pc (cf. Pier & Krolik 1992, 1993), the HINERs associated with tori are really compact emission-line regions. If the HINERs arise from the inner NLRs, the maximum dimension of the HINER is $r \sim 400 L_{43.5}^{1/2}$ pc, where $L_{43.5}$ is the ionizing luminosity in units of $10^{43.5}$ ergs s^{-1} under $n_e \sim 10^2$ cm^{-3} (Ferguson et al. 1997). Their models also suggest that the higher ionization lines tend to be more centrally concentrated; e.g., the very high-ionization lines such as [Fe XIV] λ5303 and [Fe XI] λ7892 arise from the very inner region ($r < 1$ pc), while the typical lines such as [Fe VII] λ6087 and [Fe X] λ6374 can come from $r < 100$ pc region. On the other hand, the third model suggests that typical dimensions of HINERs are of order 1 kpc (KF89).

The present study has shown that the HINER of Tololo 0109−383 is spatially extended up to 1.1 kpc in radius. Therefore, the third model is the most appropriate one for this galaxy. Although, however, KF89 considered that the most high-ionization emission lines come from extended, very low-density ($n_e \sim 1$ cm^{-3}) ISM, the majority of the

TABLE 6

HIGH-IONIZATION IRON EMISSION-LINE RATIOS

Model	Parameters	F([Fe VII] λ6087)/F([Fe X] λ6374)	F([Fe XIV] λ5303)/F([Fe X] λ6374)
KF 89[a], photoionization.....	$n_e = 1$ cm^{-3}	1.04	0.095
	$n_e = 3$ cm^{-3}	0.77	0.098
	$n_e = 10$ cm^{-3}	0.62	0.079
VAC 89[b], shock	$V_{\rm shock} = 100$ km s^{-1}	$\gg 1$	...
	$V_{\rm shock} = 300$ km s^{-1}	0.71	...
	$V_{\rm shock} = 500$ km s^{-1}	0.57	...
Observations:			
FS 83[c].....		1.47	0.62
This study		...	1.87

[a] Korista & Ferland 1989.
[b] Viegas-Aldrovandi & Contini 1989.
[c] Fosbury & Sansom 1983.

high-ionization emission lines come from the inner 440 pc region. It is noted that the electron density in the inner 440 pc region is estimated to be $n_e \sim 600[T_e/(10^4\ {\rm K})]^{1/2}$ cm^{-3}. Ferguson et al. (1997) give the maximum dimension of a HINER is $r \sim 400 L_{43.5}^{1/2}$ pc, where $L_{43.5}$ is the ionizing luminosity in units of $10^{43.5}$ ergs s^{-1} under $n_e \sim 10^2$ cm^{-3}. The *IRAS* 60 and 100 μm fluxes give a far-infrared (FIR) luminosity[4] $L_{\rm FIR} \simeq 2 \times 10^{43}$ ergs s^{-1}. Although the soft X-ray luminosity (0.5–4.5 keV) is about $L_{\rm X} \simeq 2 \times 10^{41}$ ergs s^{-1} (Green, Anderson, & Ward 1992), the bolometric luminosity is estimated to be of order 10^{43} ergs s^{-1}, taking the above FIR luminosity into account. Therefore, the observed dimension of the inner HINER is almost consistent with their expectation. On the other hand, the outer HINER region (i.e., 220 pc $< r <$ 1100 pc) is, however, interpreted by the KF89 model. This outer region also has an electron density of $n_e \sim 100[T_e/(10^4\ {\rm K})]^{1/2}$ cm^{-3}. However, this electron density is estimated using the [S II] doublet ratio, and thus it is not necessary to consider that the typical electron density in the outer HINER is the same as the above value. As discussed in § 3.3, the average electron density at $r \sim 1$ kpc is estimated to be of order 1 cm^{-3}. It is thus likely that the NLR may have density inhomogeneity more or less. If some low-density blobs in the outer NLR are exposed to the central continuum source, they would become sites of HINERs. In conclusion, the HINER in Tololo 0109−383 can be understood by the hybrid model between Ferguson et al. (1997) and KF89.

Finally, we examine whether the HINER is related to the Fe II emitting region. It is known that the majority of type 1 Seyfert galaxies with stronger Fe II emission tend to have narrower Hβ emission-line widths than those without Fe II emission (cf. Zheng & O'Brien 1990). In particular, some strong Fe II Seyfert galaxies without BLRs (e.g., I Zw 1) are classified as narrow-line Seyfert 1 galaxies (Sargent 1968; Osterbrock & Pogge 1985; Halpern & Oke 1987). Since Tololo 0109−383 shares the nature of narrow-line Seyfert 1 galaxies, it is interesting to study whether or not the Fe II emission is correlated to the high-ionization iron emission. In Figure 11, we show a diagram of Fe II λ4570/Hβ versus [Fe VII] λ6087/Hα for the Seyfert nuclei in which both the Fe II and [Fe VII] emission lines are observed (Osterbrock 1977; Phillips 1978a). It is shown that there is no clear correlation between the two ratios. It is usually considered that the optical Fe II emission comes from the warm neutral zone in the BLRs (e.g., Osterbrock 1989; Netzer 1990). Therefore, we conclude that the HINERs are not physically related to the BLRs traced by the Fe II emission.

4.2. *What is the Ionization Source of HINER?*

The spatially extended structure of the HINER in Tololo 0109−383 can be understood by the photoionization models by Ferguson et al. (1997) and Korista & Ferland (1989). In order to study further the dominant physical process in the HINER, we compare the observed high-ionization iron emission-line ratios with some mood results in Table 6. Since our spectra do not cover the wavelength region where [Fe VII] λ6087 emission is present, the observed flux ratio of [Fe VII] λ6087/[Fe X] λ6374 for Tololo 0109−383 is taken from FS83. The comparison shows that the observed [Fe VII]/[Fe X] ratio may be

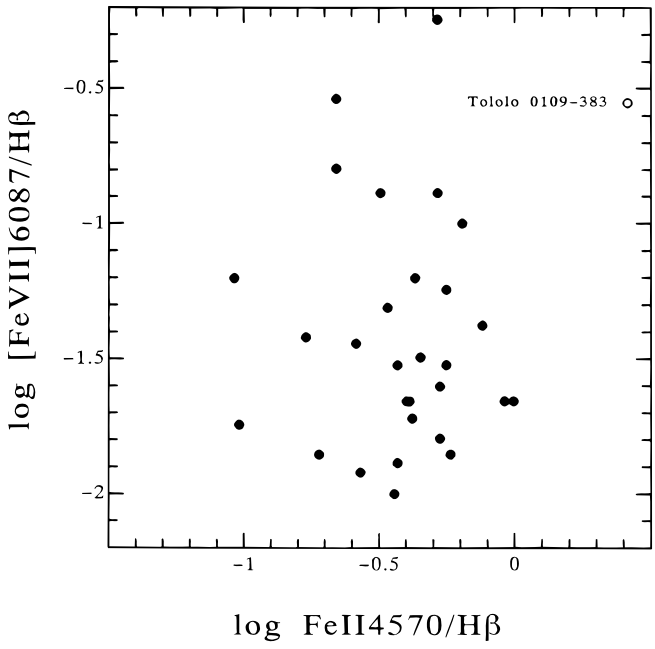

FIG. 11.—Diagram of [Fe VII] λ6087/H$\beta_{\rm broad}$ vs. Fe II λ4570/H$\beta_{\rm broad}$ for the Seyfert galaxies, in which both the [Fe VII] λ6087 and Fe II λ4570 features are unambiguously detected. The data point for Tololo 0109−383 is shown by the open circle, while the other Seyfert galaxies are shown by filled circles.

[4] The FIR luminosity is estimated using $L_{\rm FIR} = 4\pi D^2[1.25 \times 10^{-11}(2.58 S_{60\,\mu{\rm m}} + S_{100\,\mu{\rm m}})]$, where D is the distance to Tololo 0109−383 and $S_{60\,\mu{\rm m}}$ and $S_{100\,\mu{\rm m}}$ are the *IRAS* 60 and 100 μm fluxes (Jy) respectively given in the *IRAS* Faint Source Catalog (Moshir et al. 1992).

explained by both the photoionization model by KF89 and the shock model by Viegas-Aldrovandi & Contini (1989). However, the observed [Fe XIV] λ5303/[Fe X] λ6374 ratio is too high to be explained by both the models. Since, as discussed in § 3.1, the observed [Fe XIV] λ5303 line may be contaminated by the [Ca V] λ5309 emission, we do not take account of this problem seriously. However, if the unusually strong [Fe XIV] λ5303 emission is real, we would have to consider some other mechanism which can be responsible for the enhancement of this emission.

In order to study the ionization source from a statistical point of view, we examine correlations among some interesting emission-line ratios of the HINERs in Seyfert nuclei. In Figure 12, we show a diagram of emission-line ratios between [Fe X] λ6374/Hα and [Fe VII] λ6087/Hα for Seyfert 1.5 and 2 galaxies and narrow-line radio galaxies (NLRGs) (Osterbrock 1977, 1981, 1985; Koski 1978; Cohen & Osterbrock 1981; Costero & Osterbrock 1981; Cohen 1983; Shuder & Osterbrock 1981; Murayama 1995). Although the data points show a large scatter, there is a loose correlation between the two ratios. This suggests that there is a dominant, single mechanism for the ionization and excitation of these high-ionization lines. In Figure 13, we also show a diagram of emission-line ratios between [Fe VII] λ6087/Hα and [O III] λ5007/[O II] λ3727. The correlation appears better than that in Figure 10. Since the [O III] and [O II] emission lines are attributed to the photoionization by the central nonthermal continuum source, this good correlation implies tht the major ionization and excitation mechanism of the high-ionization lines is also due to the photoionization by the central nonthermal continuum source. The scatters in the diagrams (Figs. 12 and 13) suggest either that some other physical mechanisms also work for the ionization and excitation such as shocks (Viegas-Aldrovandi & Contini 1989) or that the emitting regions of HINERs are systematically different from those of intermediate-ionization lines like [O III] (Ferguson et al. 1997).

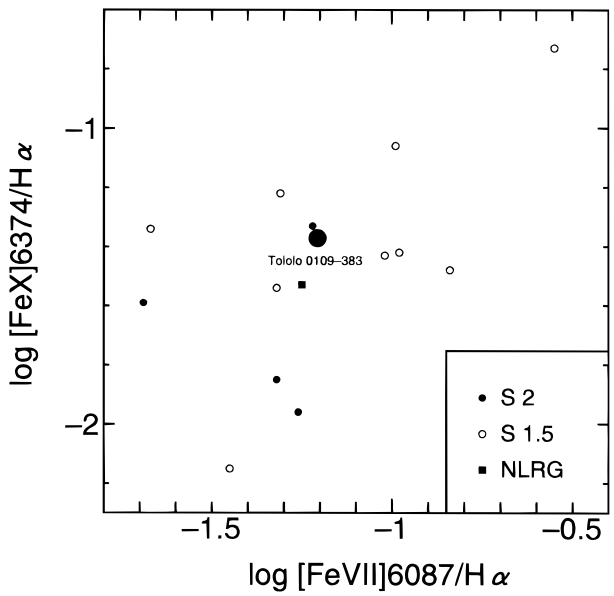

FIG. 12.—Diagram of [Fe VII] λ6087/Hα vs. [Fe X] λ6374/Hα for Seyfert galaxies. The symbols are as follows: type 2 Seyferts (*filled circle*), type 1.5 Seyferts (*filled triangle*), and narrow-line radio galaxy (*filled square*). Tololo 0109−383 is show by the big filled circle.

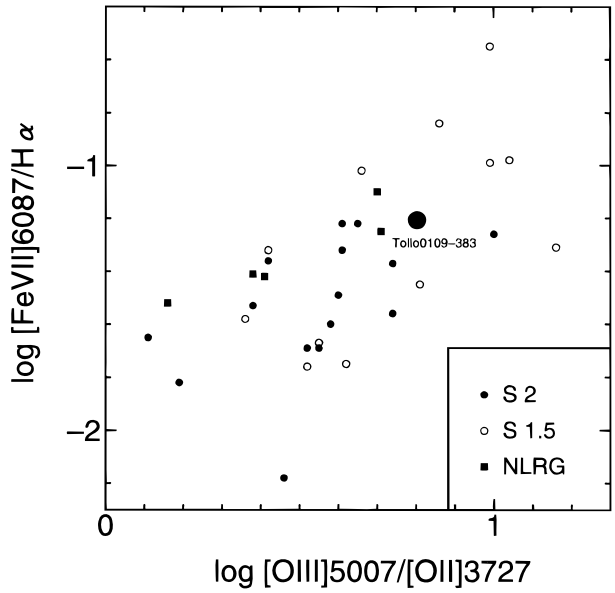

FIG. 13.—Diagram of log ([Fe VII] λ6087/Hα) vs. log ([O III] λ5007/[O II] λ3727) for Seyfert galaxies. The symbols are the same as those in Fig. 12.

Marconi et al. (1994) discussed the origin of high-ionization lines in some Seyfert nuclei as well as Tololo 0109−383 based on the near-infrared [Si VI] 1.962 μm to the optical [Fe VII] λ6087 ratio. They showed that some HINERs (e.g., IC 4329A and Mrk 463) are explained well by the photoionization of a compact (10 pc), dense ($n_e \sim 10^2$–10^6 cm^{-3}) region by a central nonthermal source with a spectral index $\alpha = -3$ to -2 (where $f_\nu \propto \nu^\alpha$). However, the HINERs of Tololo 0109−383 and the remaining Seyfert galaxies are not explained solely by the photoionization model. If we consider a possibility of shock heating again, the [Si VI]/[Fe VII] ratio (0.26) observed in Tololo 0109−383 favors relatively high-velocity shocks ($V_{\rm shock} =$ 300–500 km s^{-1}). On the other hand, the observed [Fe VII] λ6087/[Fe X] λ6374 ratio favors the low-velocity ($V_{\rm shock} <$ 100 km s^{-1}) as shown in Table 6. If the shock model would be applicable, we may take another factor into account like density inhomogeneity in the shocked region to solve this dilemma. Note that [Ca II] λλ7291, 7324 would be strong enough to be observed, if shock destroyed dust grains and brought calcium into the gas phase (Ferland 1993; Kingdon, Ferland, & Feibelman 1995; Villar-Martin & Binette 1996, 1997).

The above arguments imply that the photoionization models have more merit to explain the nature of HINERs than do the shock models. Penston et al. (1984) found that the [Fe X] emission-line fluxes of the HINERs are proportional to that of the Hβ, suggesting also that the [Fe X] emission is due to the photoionization by the central nonthermal continuum. However, the recent *Hubble Space Telescope* observations of NLRs of four type 2 Seyfert galaxies have shown that the NLRs are spatially correlated well with the radio outflows, suggesting that the shock heating is responsible for the NLRs (Capetti et al. 1996). Further, Dopita & Sutherland (1995) presented their new shock heating models, which can be responsible for the observed nature of NLRs in AGNs. The high-ionization lines will be useful in future study to understand the fundamental ionization mechanisms in AGNs.

4.3. *What is Tololo 0109−383?*

Although the basic properties of Tololo 0109−383 are quite similar to those of type 2 Seyfert galaxies, it has the following type 1 properties: (1) the presence of broad component in the Balmer emission, though its luminosity is fairly low; (2) the presence of optical Fe II features; and (3) the presence of HINER. Utilizing X-ray observations of Tololo 0109−383 and other Seyferts, we consider what is Tololo 0109−383.

Green et al. (1992) studied X-ray properties of Seyfert galaxies and quasars that have been observed (detected) by the *Einstein* and *IRAS* satellites. Both the X-ray and FIR data are available for 80 type 1 (together with quasars) and 25 type 2 Seyfert galaxies, including Tololo 0109−383. In Figure 14, we show histograms of *Einstein* IPC band (0.4–4.5 keV) to 60 μm luminosity ratio for both the type 1 and 2 Seyfert galaxies. It is shown that type 2 Seyfert galaxies have systematically smaller $L_X/L_{60\,\mu m}$ ratios than do type 1 Seyfert galaxies (Green et al. 1992). Among the type 2 Seyfert galaxies, Tololo 0109−383 has a relatively high soft X-ray–to–infrared ratio [$\log (L_X/L_{60\,\mu m}) = -2.1$].

Since nuclei in type 2 Seyfert galaxies are generally highly obscured, photoelectric absorption due to the obscuration strongly attenuates soft X-ray emission from a central source. The optical depth of the obscuration implied from a column density (N_H) could therefore be important for observed soft X-ray intensity, i.e., if the absorption column exceeds $N_H \sim 10^{23}$ cm^{-2}, no direct radiation from a central source but weak scattered light and thermal emission from a starburst or galaxy halo is visible in the soft X-ray (*Einstein*) band (e.g., Iwasawa 1995; Polletta et al. 1996). We thus compile column density measurements from hard X-ray spectroscopy of type 2 Seyfert galaxies from the literature to compare with the $L_X/L_{60\,\mu m}$ ratios (Table 7). The type 2 Seyfert galaxies with a large $L_X/L_{60\,\mu m}$ ratio tend to have absorption columns less than $N_H \simeq 10^{23}$ cm^{-2}. On the other hand, strongly absorbed objects have small $L_X/L_{60\,\mu m}$ (i.e., Mrk 3 and NGC 4507). This can be understood in terms of attenuation of direct soft X-ray emission due to absorption. The smaller the absorption column, the more softly X-rays penetrate through the obscuration to make a larger $L_X/L_{60\,\mu m}$, while $L_X/L_{60\,\mu m}$ for a starburst component can be assumed to be approximately constant

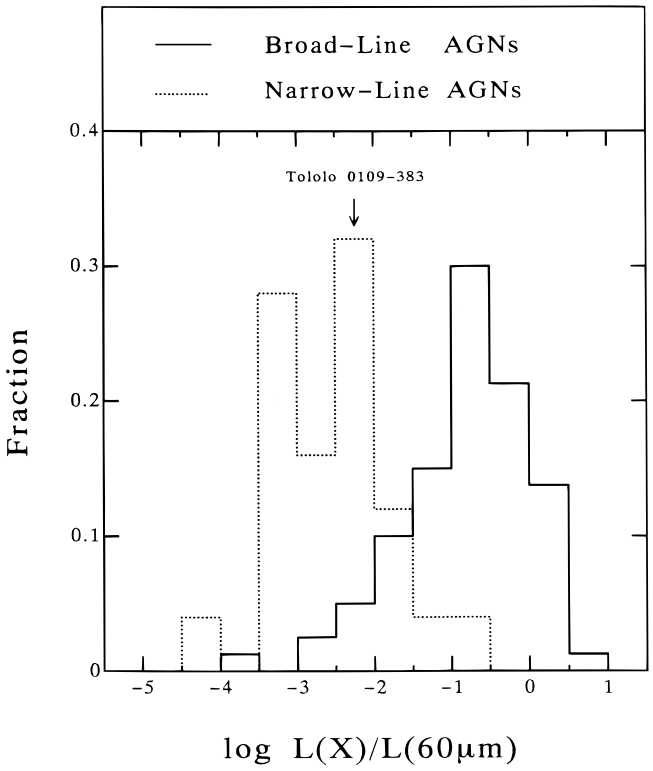

FIG. 14.—Histograms of log ($L_X/L_{60\,\mu m}$) for type 1 and type 2 AGNs. The ordinate is the relative fraction for each type of AGNs.

TABLE 7

X-RAY LOUDNESS AND ABSORPTION COLUMN DENSITY OF TYPE 2 SEYFERT GALAXIES

Object	log ($L_X/L_{60\,\mu m}$)	log N_H (cm^{-2})	Reference
NGC 2992	−0.96	21.4 ± 0.2	1
NGC 5506	−1.02	22.4 ± 0.1	1
NGC 2110	−1.60	22.4 ± 0.1	1
NGC 7496	−1.99	21.6 ± 0.6	2
Tololo 0109−393	−2.01	...	...
NGC 5674	−2.15	22.7 ± 0.1	2
Mrk 78	−2.23	...	3
Mrk 348	−2.31	23.0 ± 0.1	1
Mrk 3	−2.33	23.8 ± 0.1	1
Mrk 573	−2.41	...	3
NGC 4507	−2.52	23.7 ± 0.1	1
NGC 7582	−2.64	23.7 ± 0.1	4
NGC 4388	−2.88	23.6 ± 0.1	5
Mrk 463E	−2.90	23.4 ± 0.2	3, 6
NGC 1068[a]	−3.00	>25	1, 7
Mrk 273	−3.37	...	3
Arp 220	−4.38	...	3

[a] Direct continuum is invisible and thus the detected hard X-ray emission is interpreted as the scattered radition and hot gas from the circumnuclear starburst (Awaki et al. 1991).

REFERENCES.—(1) Goodrich, Veilleux, & Hill 1994; (2) Iwasawa et al. 1994; (3) Awaki 1992; (4) Warwick et al. 1993; (5) Iwasawa 1995; (6) Ueno et al. 1996; (7) Matt et al. 1997.

(Griffiths & Padovani 1990). Although there has been no hard X-ray observation of Tololo 01909−383, forthcoming *ASCA* observations will provide information on the obscuration in the nucleus. Let us consider a dusty/molecular torus with an inner radius, a, an outer radius, b, a height, h, and a gas mass, $M_{\rm gas}$. If we adopt $a = 1$ pc, $b = 10$ pc, $h = 2$ pc, and $M_{\rm gas} = 10^5\ M_\odot$ (see Pier & Krolik 1992, 1993), we obtain an H I column density, $N_{\rm H\,I} \sim 2 \times 10^{23}\ [M_{\rm gas}/(10^5\ M_\odot)][b/10\ {\rm pc})]^{-1}[h/(2\ {\rm pc})]^{-1}\ {\rm cm}^{-2}$ for an edge-on view toward the torus. Thus it is considered that type 2 Seyferts blocked by such tori are observed as X-ray quiet type 2 Seyferts. On the other hand, if either the blocking by the tori is incomplete because of some irregular density distribution within the tori; if we observe the central engine from a more favorable angle, some type 2 Seyfert galaxies are observed as X-ray loud ones, although the BLRs are still hidden by the tori. We consider that Tololo 0109−383 is a member of the latter class of type 2 Seyferts, though it is the marginal Seyfert galaxy between type 1 and 2.

We would like to thank the staff of Cerro Tololo Inter-American Observatory, and in particular, Mark Phillips and Mario Hamuy, for their kind guidance and useful suggestions regarding the observations. We wish to thank Kentaro Aoki for insightful comments and discussions. We also thank Kojun Yamashita, Katsuji Koyama, Yuzuru Tawara, and Hideyo Kunieda for encouragement. We are grateful to the referee, Gary Ferland, for his useful comments. K. I. thanks PPARC and the Ministry of Education, Science, Sports, and Culture for financial support. T. M. was supported by the Grant-in-Aid for JSPS Fellows by the Ministry of Education, Science, Sports, and Culture of Japan.

REFERENCES

Alloin, D., Bica, E., Bonatto, C., & Prugniel, P. 1992, A&A, 266, 117
Awaki, H. 1992, in Frontiers of X-ray Astronomy, ed. Y. Tanaka & K. Koyama (Tokyo: Universal Acad.), 537
Awaki, H., Koyama, K., Inoue, H., & Halpern, J. P. 1991, PASJ, 43, 195
Bergeron, J., & Kunth, D. 1980, A&A, 85, L11
Boisson, C., & Durret, F. 1986, A&A, 168, 32
Capetti, A., Axson, D. J., Macchetto, F., Sparks, W. B., & Boksenberg, A. 1996, ApJ, 469, 554
Cohen, R. D. 1983, ApJ, 273, 489
Cohen, R. D., & Osterbrock, D. E. 1981, ApJ, 243, 81
Costero, R., & Osterbrock, D. E. 1977, ApJ, 211, 675
Dahari, O., & De Robertis, M. M. 1988, ApJ, 331, 727
De Robertis, M. M., & Osterbrock, D. E. 1984, ApJ, 286, 171
———. 1986, ApJ, 301, 727
de Vaucouleurs, G., de Vaucouleurs, A., Corwin, H. C., Jr., Buta, R. J., Paturel, G., & Fouqué, P. 1991, Third Reference Catalogue of Bright Galaxies (New York: Springer)
Dopita, M. A., & Sutherland, R. S. 1995, ApJ, 455, 468
Durret, F. 1990, A&A, 229, 351
Durret, F., & Bergeron, J. 1987, A&A, 173, 219
———. 1988, A&AS, 75, 273 (DB88)
Feldman, F. R., Weedman, D. W., Balzano, V. A., & Ramsay, L. W. 1982, ApJ, 256, 427
Ferguson, J. W., Korista, K. T., & Ferland, G. J. 1997, ApJS, 110, 287
Ferland, G. J. 1993, in The Nearest Active Galaxies, ed. J. E. Beckman, L. Colina, & H. Netzer (Madrid: CSIC), 75
Ferland, G. J., & Netzer, H. 1983, ApJ, 264, 105
Ferland, G. J., & Osterbrock, D. E. 1985, ApJ, 289, 105
———. 1986, ApJ, 300, 658
Filippenko, A. V. 1985, ApJ, 289, 475
Fosbury, R. A. E., & Sansom, A. E. 1983, MNRAS, 204, 1231 (FS83)
Golev, V., Yankulova, I., Bonev, T., & Jockers, K. 1994, Astrophys. Lett. Comm., 29, 239
Goodrich, R. W., Veilleux, S., & Hill, G. J. 1994, ApJ, 422, 521
Grandi, S. A. 1978, ApJ, 221, 501
Green, P. J., Anderson, S. F., & Ward, M. J. 1992, MNRAS, 254, 30
Griffiths, R. E., & Padovani, P. 1990, ApJ, 360, 483
Halpern, J. P., & Oke, J. B. 1987, ApJ, 312, 91
Hamuy, M., Walker, A. R., Suntzeff, N. B., Gigoux, P., Heathcote, S. R., & Phillips, M. M. 1992, PASP, 104, 533
Heckman, T. M. 1980, A&A, 87, 152
Iwasawa, K. 1995, Ph. D. thesis, Nagoya Univ.
Iwasawa, K., Kunieda, H., Tawara, Y., Awaki, H., Koyama, K., Murayama, T., & Taniguchi, Y. 1995, AJ, 110, 551
Iwasawa, K., Yaqoob, T., Awaki, H., & Ogasaka, Y. 1994, PASJ, 46, L167
Joly, M. 1991, A&A, 242, 49
Kingdon, J., Ferland, G. J., & Feibelman, W. A. 1995, ApJ, 439, 793
Korista, K. T., & Ferland, G. J. 1989, ApJ, 343, 678 (KF89)
Koski, A. T. 1978, ApJ, 223, 56
Kunth, D., & Sargent, W. L. W. 1979, A&A, 76, 50
Lauberts, A. 1982, The ESO/Uppsala Survey of the ESO(B) Atlas (Munich: ESO)
Lawrence, A., Saunders, W., Rowan-Robinson, M., Crawford, J., Ellis, R., Frenk, C. S., Efstathiou, G., & Kaiser, N. 1988, MNRAS, 235, 261
Lipari, S., Terlevich, R., & Macchetto, F. 1993, ApJ, 406, 451
Marconi, A., Moorwood, A. F. M., Salvati, M., & Oliva, E. 1994, A&A, 291, 18
Matt, G., et al. 1997, A&A, 325, L13
Moshir, M., et al. 1992, Explanatory Supplement to the IRAS Faint Source Survey (Version 2; Pasadena: JPL)
Murayama, T. 1995, Master's thesis, Tohoku Univ.
Netzer, H. 1974, MNRAS, 169, 579
Netzer, H. 1990, in Active Galactic Nuclei, ed. T. J.-L. Courvoisier & M. Major (Springer-Verlag), 98
Nussbaumer, H., & Osterbrock, D. E. 1970, ApJ, 161, 811
Oke, J. B., & Sargent, W. L. W. 1968, ApJ, 151, 807
Oliva, E., Salvati, M., Moorwood, A. F., M., & Marconi, A. 1994, A&A, 288, 457
Osterbrock, D. E. 1969, Astrophys. Lett., 4, 57
———. 1977, ApJ, 215, 733
———. 1981, ApJ, 246, 696
———. 1989, Astrophysics of Gaseous Nebulae and Active Galactic Nuclei (San Francisco: Freeman)
Osterbrock, D. E., & Pogge, R. W. 1985, ApJ, 297, 166
Pelat, D., Alloin, D., & Fosbury, R. A. E. 1981, MNRAS, 195, 787
Penston, M. V., Fosbury, R. A. E., Boksenberg, A., Ward, M. J., & Wilson, A. S. 1984, MNRAS, 208, 347
Peterson, B. M. 1993, PASP, 105, 247
Phillips, M. M. 1978a, ApJS, 38, 187
———. 1978b, ApJ, 226, 736
Pier, E., & Krolik, J. 1992, ApJ, 401, 99
———. 1993, ApJ, 418, 673
Pier, E. A., & Voit, M. G. 1995, ApJ, 450, 628
Polletta, M., Bassani, L., Malaguti, G., Palumbo, G. G. C., & Caroli, E. 1996, ApJ, 106, 399
Sargent, W. L. W. 1968, ApJ, 152, L31
Schmitt, H. R., & Kinney, A. 1996, ApJ, 463, 498
Shuder, J. M., & Osterbrock, D. E. 1981, ApJ, 250, 55
Smith, M. G. 1975, ApJ, 202, 591
Ueno, S., Koyama, K., Awaki, H., Hayashi, I., & Blanco, P. R. 1996, PASJ, 48, 389
Ueno, S., Mushotzky, R. F., Koyama, K., Iwasawa, K., Awaki, H., & Hayashi, I. 1994, PASJ, 46, L71
Ulvestad, J. S., & Wilson, A. S. 1989, ApJ, 343, 659
Veilleux, S. 1991, ApJ, 368, 158
Veilleux, S., & Osterbrock, D. E. 1987, ApJS, 63, 295
Viegas-Aldrovandi, S. M., & Contini, M. 1989, A&A, 215, 253
Villar-Martin, M., & Binette, L. 1996, A&A, 309, 97
———. 1997, A&A, 317, 350
Warwick, R. S., Sembey, S., Yaqoob, T., Makishima, K., Ohashi, T., Tashiro, M., & Kohmura, Y. 1993, MNRAS, 265, 412
Zheng, W., & O'Brien, P. T. 1990, ApJ, 353, 433